NeuroImage 155 (2017) 490–502

Contents lists available at ScienceDirect

NeuroImage

journal homepage: www.elsevier.com/locate/neuroimage

Transient networks of spatio-temporal connectivity map communication pathways in brain functional systems

Alessandra Griffa[a,b,*], Benjamin Ricaud[c], Kirell Benzi[c], Xavier Bresson[c], Alessandro Daducci[b], Pierre Vandergheynst[c], Jean-Philippe Thiran[a,b], Patric Hagmann[a,b]

[a] Department of Radiology, Centre Hospitalier Universitaire Vaudois (CHUV) and University of Lausanne (UNIL), Lausanne 1011, Switzerland
[b] Signal Processing Laboratory 5 (LTS5), École Polytechnique Fédérale de Lausanne (EPFL), Lausanne 1015, Switzerland
[c] Signal Processing Laboratory 2 (LTS2), École Polytechnique Fédérale de Lausanne (EPFL), Lausanne 1015, Switzerland

ARTICLE INFO

Keywords:
Resting-state fMRI
Diffusion MRI
Brain connectivity
Multilayer network
Temporal network
Brain dynamics
Point-process
Communication-through-coherence
Spatio-temporal connectome

ABSTRACT

The study of brain dynamics enables us to characterize the time-varying functional connectivity among distinct neural groups. However, current methods suffer from the absence of structural connectivity information. We propose to integrate infra-slow neural oscillations and anatomical-connectivity maps, as derived from functional and diffusion MRI, in a multilayer-graph framework that captures transient networks of spatio-temporal connectivity. These networks group anatomically wired and temporary synchronized brain regions and encode the propagation of functional activity on the structural connectome. In a group of 71 healthy subjects, we find that these transient networks demonstrate power-law spatial and temporal size, globally organize into well-known functional systems and describe wave-like trajectories of activation across anatomically connected regions. Within the transient networks, activity propagates through polysynaptic paths that include selective ensembles of structural connections and differ from the structural shortest paths. In the light of the communication-through-coherence principle, the identified spatio-temporal networks could encode communication channels' selection and neural assemblies, which deserves further attention. This work contributes to the understanding of brain structure-function relationships by considering the time-varying nature of resting-state interactions on the axonal scaffold, and it offers a convenient framework to study large-scale communication mechanisms and functional dynamics.

Introduction

In the human brain, a functional system refers to a set of interconnected brain regions involved in the treatment of a specific task, that can be perceptual, motoric, cognitive or emotional (Laird et al., 2009). Functional systems show a large variety of brain activation patterns (Park and Friston, 2013), adapt to different conditions (Bassett et al., 2013; Braun et al., 2015; Spadone et al., 2015), interact dynamically (Cocchi et al., 2013) and demonstrate coherent (Smith et al., 2009) but non-stationary (Hutchison et al., 2013) behavior at rest. Indeed, a key aspect of the brain is its ability to adapt to multiple conditions through context-dependent interactions among neuronal units. The functional response to external and internal demands requires a flexible coupling of different brain units that are structurally connected through a complex but fixed axonal network (Bullmore and Sporns, 2012; De Pasquale et al., 2015; Deco et al., 2015). This process necessarily involves an efficient and context-dependent selection of structural communication channels among multiple possible structural paths. It has been advocated that the specific architecture of the whole-brain structural network (or connectome) is optimized for, and supports efficient communication and flexible switching among discrete functional states (Senden et al., 2014; Ponce-Alvarez et al., 2015; Hellyer et al., 2015; Goñi et al., 2013; Honey et al., 2010). However how functional interactions unfold through the structural connectome has been only partially investigated, and our understanding of large-scale brain communication processes remain limited. In this work we introduce a new methodological framework based on multilayer-graph formalism to follow the propagation of time-dependent functional patterns through viable structural pathways for communication. The multilayer graph combines structural connectivity information estimated from diffusion magnetic resonance imaging (dMRI) and functional dynamics derived from resting-state functional MRI (rs-fMRI).

The brain functional connectivity, i.e. the statistical dependency between the oscillations of brain units, has been widely investigated by

* Correspondence to: Service de Radiodiagnostic et Radiologie Interventionnelle - BH Bugnon 46, CH-1011 Lausanne, Switzerland.
E-mail address: alessandra.griffa@epfl.ch (A. Griffa).

http://dx.doi.org/10.1016/j.neuroimage.2017.04.015
Received 13 February 2017; Accepted 6 April 2017
Available online 12 April 2017

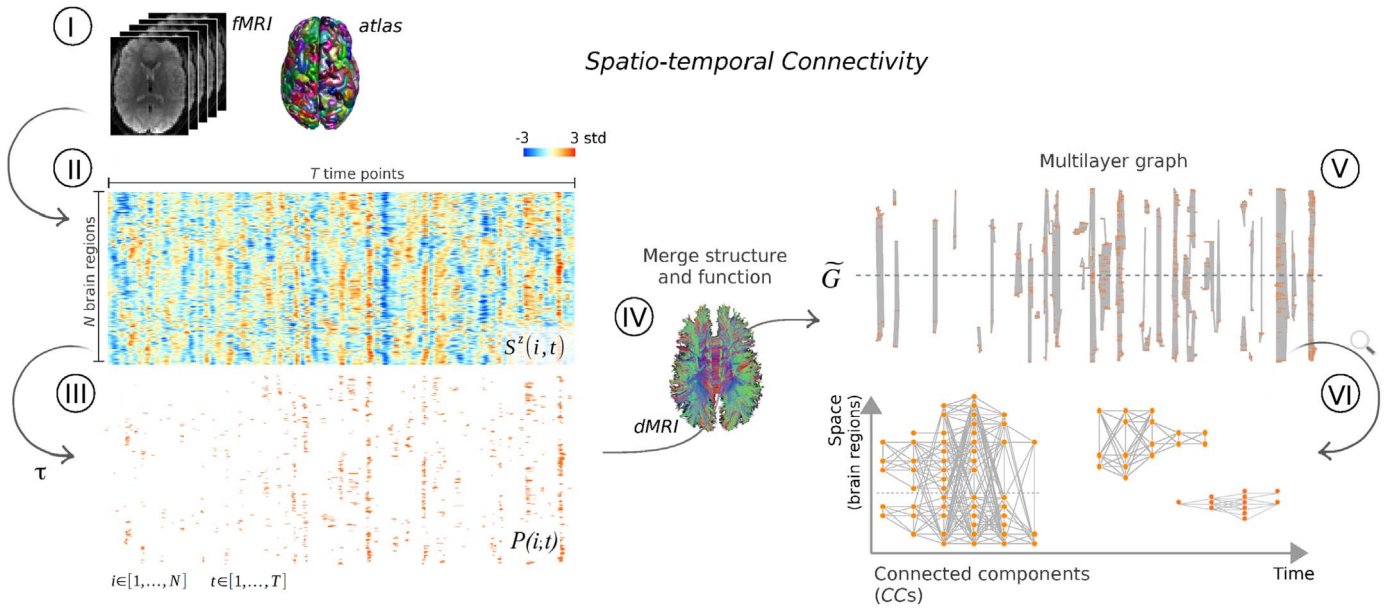

Fig. 1. Construction of a spatio-temporal connectome. (I) The cortical brain volume is segmented into N regions of interest according to a given atlas. Each brain region is associated with an average functional time series of length T time points derived from fMRI data. (II) Regional fMRI time series are z-scored and represented in the figure as a matrix $S^z(i,t)$ of size NxT ($\in[1,\ldots,N]$, $t\in[1,\ldots,T]$). (III) The z-scored fMRI time series are reduced to binary point-processes by applying a threshold τ. The elements of the resulting matrix $P(i,t)$ represent the active or quiescent status of the brain region i at time point t. A multilayer graph $\widetilde{G}$ is then constructed by merging the point-processes and the anatomical connectivity information derived from dMRI tractography (IV). (V) Each node of $\widetilde{G}$ represents a specific brain region at a given time point; two nodes are connected in $\widetilde{G}$ if (i) they are co-active at the same or neighboring time points AND (ii) they are linked by a white matter tract. In panel (V) the nodes of $\widetilde{G}$ are pictured in orange and the edges in grey; disconnected nodes and edge directionality are not shown. The weakly connected components (*CC*s) of the multilayer graph extend spatially (across different brain regions) and temporally (over multiple time points) and represent transient networks of spatio-temporal connectivity. Panel (VI) show a zoom of some representative *CC*s of $\widetilde{G}$.

means of rs-fMRI studies that highlight the modular structure of the brain architecture and decompose it into a set of reproducible resting state networks (RSNs) (Damoiseaux et al., 2006; Fox et al., 2005; Yeo et al., 2011). Although traditional approaches implicitly assume that the resting-state activity is stationary over an fMRI recording, an increasing effort has been devoted to the characterization of resting-state dynamics (Hutchison et al., 2013; Calhoun et al., 2014). In this regards two main methodological directions can be identified: temporal sliding window approaches, or time-resolved investigation of short functional events through point-process analysis (i.e., thresholding of fMRI signals) or regularized deconvolution methods (Hutchison et al., 2013; Preti et al., 2017). While sliding-window approaches are a natural extension of more traditional functional connectivity analyses, they posit methodological challenges in terms of balance between window selection and temporal resolution of observed dynamics (Leonardi and Van De Ville, 2015; Zalesky and Breakspear, 2015; Telesford et al., 2016). On the other side, methods detecting short functional events require a certain degree of parameter tuning and relies on the conceptualization of resting-state dynamics as sparse sequence of key functional activations (Petridou et al., 2013; Tagliazucchi et al., 2016). Both approaches have delivered qualitatively comparable findings (Preti et al., 2017), showing that at short temporal scales functional patterns can significantly diverge from classical RSNs (Allan et al., 2015; Hutchison et al., 2013). During a resting-state period, the brain might explores a space of states (functional configurations persisting for a transient but sufficiently long periods of time (Kitzbichler et al., 2009; Calhoun et al., 2014)) with cortical areas engaging and disengaging in variable functional subnetworks (Liu and Duyn, 2013; Zalesky et al., 2014; Betzel et al., 2016). These dynamics give rise to complex (and possibly temporally and spatially overlapping) patterns of interaction (Karahanoğlu and Van De Ville, 2015), which have been related to behavioral variables (Chang et al., 2016) and cognitive processes (Bassett et al., 2011; Chen et al., 2015).

Conceptually, the transient functional couplings observed in resting-state dynamics can be associated with time-dependent communication processes. At the mesoscopic scale it has been proposed that transient patterns of temporal coherence, among the electrical oscillations of structurally wired neural groups, provide temporal windows for effective communication and implement mechanisms of selective information processing (Fries, 2005). This communication-through-coherence (CTC) mechanism pertains to neural coupling in the gamma and beta frequency bands (Fries, 2005, 2015), but might be reflected at the coarser spatial and temporal scales accessible with magnetic resonance imaging (MRI) (Deco and Kringelbach, 2016). Crucially, the CTC hypothesis explicitly relates the transient functional coupling between wired nervous regions with their inter-communication and efficient information flow.

In the present study we develop a framework that captures resting-state interactions among anatomically connected brain regions in the form of transient network of spatio-temporal connectivity. Specifically, we define a spatio-temporal connectome as a multilayer graph (Kivelä et al., 2014) that specifies node proximity both in the temporal and in the spatial domains. On one hand, proximity in time is expressed by time-resolved co-activation of brain regions at neighboring time points, as detected through a point-process analysis of rs-fMRI time series. On the other hand, anatomical proximity is expressed by brain regions' adjacency in the structural connectome, as estimated from dMRI tractography. The weakly connected components of the resulting multilayer graph conveniently represent time-dependent events of synchronous activation among anatomically wired regions, a possible expression of brain communication processes. After the methodological description of the spatio-temporal connectome framework, we explore its feasibility through synthetic data and we introduce different measures for the characterization of the connected components of the multilayer graph. These connected components reveal time-varying pathways of activity propagation and, by being clustered, identify reproducible patterns of spatio-temporal connectivity across fMRI recordings and across multiple subjects. We report on the organization of these patterns, and we investigate their internal dynamics. We discuss the relevance of considering functional dynamics in combination with the underlying structural wiring to study large-scale brain communication mechanisms and activity propagation routing.

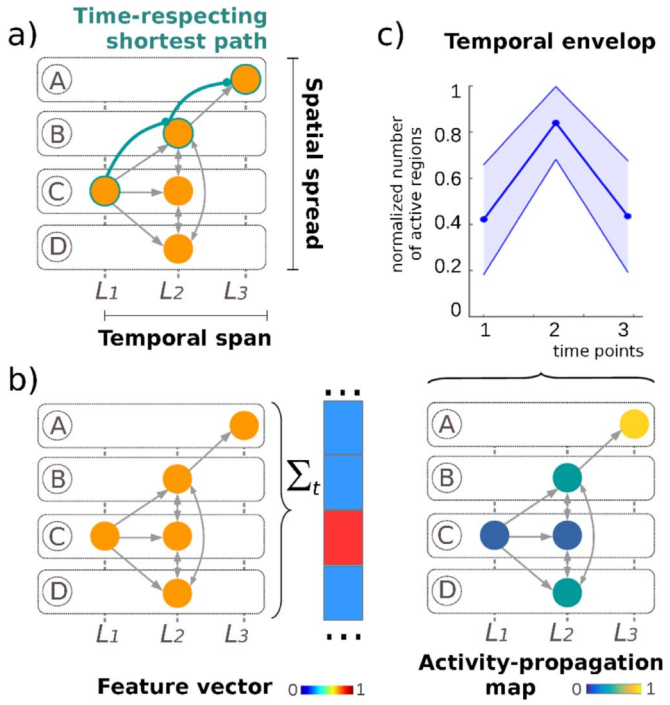

Fig. 2. Connected components (*CC*s) characterization. Each panel of the figure represents a *CC* toy example. The nodes of the *CC* are pictured in orange; each node represents a cortical brain region (A, B, C or D) at a particular time point (layer L_1, L_2 or L_3 of a multilayer graph). (a) Schematic representation of the *CC*' s temporal span and spatial spread. A time-respecting shortest path of length 2, from node (*C,1*) to node (*A,3*), is represented in green. (b) A *CC* is reduced to a feature vector of length *N* (*N* total number of brain regions) by integration along the temporal axis and normalization by the vector's l2-norm. (c) Spatio-temporal behavior of the *CC*s. The *CC*'s temporal envelop represents the normalized number of brain regions active at each time point. The *CC*'s activity-propagation map represents the average normalized time point at which each brain region is active within the *CC*: blue regions are active before yellow regions.

Materials and methods

Materials and Methods are organized as follows. In Section 2.1 we describe in details the methodological steps for the construction of a spatio-temporal connectome from resting-state fMRI and dMRI data. Related Python code is publicly available at https://github.com/agriffa/STConn. A spatio-temporal connectome is a multilayer graph embedding transient networks of spatio-temporal connectivity. In Section 2.2 we discuss the general assumptions underlying the proposed spatio-temporal framework and describe relevant tests on surrogate data. In Section 2.3 we introduce relevant measures to characterize the spatial topology and temporal evolution of the transient networks of spatio-temporal connectivity. The methodology and the measures of spatio-temporal connectivity are summarized in Figs. 1 and 2. Finally, in Section 2.4 we provide details on the experimental data considered in this study including MRI data acquisition, processing pipelines and spatio-temporal connectome analysis.

Spatio-temporal connectomics

We propose to represent brain functional dynamics and structural connectivity information in the form of a particular multilayer graph (Benzi et al., 2016; Kivelä et al., 2014), named spatio-temporal connectome. Intuitively, a spatio-temporal connectome is made of layers of nodes bound together by intra- and inter-layer edges representing instantaneous functional relationships between anatomically connected brain regions. Each layer of the graph corresponds to a single time point of a functional neuroimaging experiment and its nodes represent distinct brain regions at a specific time point. Two nodes are connected in the multilayer graph if the corresponding brain regions are (1) anatomically wired and (2) functionally co-active at the same time point (intra-layer edges) or at two following time points (inter-layer edges) (Fig. 1).

Structural connectivity

The overall set of white matter tracts connecting cortical region pairs can be represented as a single-layer, structural connectivity graph *G(V,E)*. *V* is the set of vertices of *G*, with $|V|=N$ number of cortical regions. $E=\{(i,j)|i,j\in V\}$ is the set of undirected edges. The structural graph *G* is estimated by combining dMRI tractography and a suitable parcellation of the cortical volume (Bullmore and Sporns, 2009; Hagmann et al., 2008). Note that in the general case *G* can be weighted but in the present work we model structural connectivity as a binary graph only.

Time-resolved functional connectivity and point-process analysis

FMRI measures blood oxygenation level dependent (BOLD) signals related to neuronal and vascular changes. Under the assumption of linearity the BOLD signal is understood as the convolution of a series of local neural events with a hemodynamic response function (HRF) (Lindquist, 2008). Different methods have been proposed to retrieve temporal sequences of spontaneous activations from fMRI data, including high-amplitude event analysis (or point-process analysis) and spatio-temporally regularized deconvolution of BOLD signals (Tagliazucchi et al., 2012; Karahanoğlu et al., 2013). In this work we use a point-process analysis to reduce regional BOLD signals to binary processes describing whether a cortical region is active or quiescent at a particular time point. Accordingly, the BOLD signals are z-scored and a threshold is applied to identify the binary sequences of high-amplitude events. Formally, we denote by S^z the matrix collecting the z-scored fMRI time series associated with *N* cortical regions (Fig. 1, panels I and II). $S^z(i,\ t)$ is the z-scored fMRI value at region i ($i\in[1,\ \ldots,\ N]$) and time point t ($t\in[1,\ \ldots,\ T]$), with *T* number of time points of the fMRI recording. The point-process matrix *P* is given by applying to S^z a positive threshold τ: $P(i,\ t)=1 if S^z(i,\ t)\geqslant\tau; P(i,\ t)=0 otherwise$ (Fig. 1, panel III). *P* has dimensions *NxT* and *P(i,t)* represents the functional status (active or quiescent) of region *i* at time point *t*.

Multilayer graph construction

We build a multilayer graph $\widetilde{G}$, named spatio-temporal connectome, by merging the anatomical connectivity information (*G*) and the local activity processes (*P*) (Fig. 1). The multilayer graph $\widetilde{G}$ is made of *T* layers $\{L_1, L_2, \ldots, L_T\}$ representing single time points of the fMRI experiment. Each layer contains *N* nodes corresponding to distinct cortical regions, for a total of *NxT* nodes. Note that the *N* nodes contained in each layer of $\widetilde{G}$ are as well vertices of the single-layer structural graph *G*. We denote by i_t the node of layer L_t associated with the cortical region *i* (vertex *i* on *G*). Two nodes i_t, j_t belonging to the same layer L_t of $\widetilde{G}$ are connected if (1) $(i,\ j)\in E$(regions *i* and *j* are adjacent in *G*) and (2) *P(i,t) = P(j,t) = 1* (regions *i* and *j* are both active at time point *t*). Two nodes i_t, j_{t+1} belonging to two following layers L_t, L_{t+1} of $\widetilde{G}$ are connected if (1) $(i,\ j)\in E$(regions *i* and *j* are adjacent in *G*) and (2) *P(i,t) = P(j,t+1) = 1* (regions *i* and *j* are active at two following time points *t, t+1*). Indeed, one can also view this multilayer graph as a particular type of temporal graph, which naturally adds information about time of interactions (Holme and Saramaki, 2012). We note that intra-layer edges (i_t, j_t) are bi-directed, as it is not possible to establish the sequentiality of functional events occurring in a time window shorter than the temporal resolution of the fMRI recording. Inter-layer edges (i_t, j_{t+1}) are uni-directed, and the edges' directionality is implied by the temporal ordering of the layers. The resulting multilayer graph is highly sparse and counts a series of distinct weakly connected components (*CC*s). Fig. 1, panel V represents the multilayer

graph of a single example subject; Fig. 1, panel VI provides a zoom of two examples of connected components in the same multilayer graph.

Framework hypotheses and validation

The proposed multilayer framework explicitly links functional co-activations of anatomically connected brain regions allowing to following the propagation of brain dynamics on the structural connectome. As such, the framework relies on two implicit hypotheses. The first hypothesis is that the synchronization of high-amplitude fMRI events represents transient functional interactions (or time-resolved functional connectivity) between distinct brain regions. The second hypothesis is that the most significant functional interactions taking place at the temporal scale of seconds (which is the typical fMRI temporal resolution) occur between anatomically connected brain regions. In this section we provide dedicated analyses on surrogate data in support of these hypotheses.

Synchronization of high-amplitude fMRI events

In this work we assume that the synchronization of high-amplitude fMRI events (or functional co-activations) represents transient functional interactions between distinct brain regions.

As a first sanity check, we questioned whether the number of functional co-activations detected in resting-state fMRI data is higher than what would be expected by chance. To this end we generated a set of surrogate time series by independently phase-randomizing the regional fMRI signals, similarly to Handwerker et al. (2012), Karahanoğlu and Van De Ville (2015). This method consists in randomly shuffling the Fourier phases of the *N* fMRI time series and generates uncorrelated data with preserved autocorrelation properties (Theiler et al., 1992).

Furthermore, we questioned whether the functional co-activations detected in resting-state fMRI data are completely explained by the linear relationship between region pairs, or if they can be partly ascribed to time-varying relationships between region pairs. To this end we compared the number of functional co-activation in the original data with the number of co-activations in surrogate data with preserved static functional connectivity. We generated surrogate time series by uniformly phase-randomizing the regional fMRI time series, similarly to Allen et al. (2012), Hindriks et al. (2016). This method consists of adding the same random phase sequence to the Fourier phases of all the *N* fMRI time series, thus preserving the autocorrelation and cross-correlation properties of the multivariate process (Prichard, 1994). As an alternative test, we also evaluated the contribution of time-varying fMRI relationships on co-activation patterns by signals orthogonalization. The orthogonalization of one signal with respect to a second one removes the contribution of their linear correlation (static functional connectivity) on the co-activation patterns. For a given fMRI dataset, we considered each pair of regional time series, orthogonalized the two using the Gram-Schmidt process and computed the number of co-activations between the orthogonalized signals. We repeated this procedure for all the *N*x*N* fMRI signal pairs.

An example of experimental fMRI, surrogate (independent and uniform phase-randomization) and orthogonalized time series is shown in Fig. 3. Inline Supplementary Figure S1 shows the cross-correlation matrices for the same data. To test experimental data against surrogate and orthogonalized null-models we compared the total number of co-activations among the different cases, for all pairs of brain regions.

Functional interactions and anatomical connectivity

In a spatio-temporal connectome two brain regions are connected if they are functionally co-active and anatomically wired, allowing to following the propagation of functional dynamics on the structural connectome. This double constraint discards from further analyses time-resolved co-activations between disconnected brain regions. It relates to the implicit hypothesis that the most significant time-resolved activity (inferred from fMRI recordings) propagates through structural pathways. To question this hypothesis we compared the reproducibility of time-resolved functional co-activations between anatomically connected and unconnected region pairs, over time and across independent fMRI acquisitions. We expect that the most significant functional interactions will be consistently detected in multiple fMRI data and subjects.

Given a set of spatio-temporal connectomes from multiple subjects, we first counted the recurrence of functional co-activations between each pair of structurally connected cortical regions (edges of the spatio-temporal connectomes). Second, we counted the recurrence of co-activations taking place outside the *CC*s of the spatio-temporal connectomes. This information can be summarized in two non-symmetric matrix of size *N*x*N*. We evaluated and compared the distributions of the pairwise co-activations between connected and unconnected regions pairs.

Transient networks of spatio-temporal connectivity

A spatio-temporal connectome constructed according to the above-described methods is a multilayer graph, which is sparse both in time and space. The weakly connected components of the multilayer graph (Kivelä et al., 2014) can be interpreted as transient networks of spatio-temporal connectivity. They encode the spreading of functional events among anatomically connected brain regions, at specific time instant and across successive frames. We introduce a set of measures for the characterization of the *CC*s and the associated brain dynamics, in relation to the following dimensions: duration, spatial extension and structural pathways within the *CC*s; spatial maps of activation; spatio-temporal propagation of functional activity.

Connected components characterization and time-respecting paths

The temporal span and the spatial spread of the *CC*s provide the basic spatio-temporal characteristics of the transient spatio-temporal events (Fig. 2a). We define the temporal span of a *CC* as the length of the temporal window over which the component is active. The spatial spread of a *CC* is the number of brain regions that are active within the component. Each *CC* includes several time-respecting paths between active brain regions, which represent viable structural pathways of functional activity propagation. The concept of time-respecting paths is related to temporal network theory (Holme and Saramaki, 2012). When considering a source node i_t and a destination node j_{t+k} ($k \geqslant 0$) of $\widetilde{G}$, the time-respecting path from i_t to j_{t+k} is an ordered sequence of connected nodes with non-decreasing time indexes. In our framework, the length of a time-respecting path is defined as the number of distinct brain regions visited along the path (or number of hops between the source and destination brain regions) (see Inline supplementary Methods, *Spatio-temporal connectomics and temporal graphs*) (Fig. 2a). The time-respecting distance $d_{tr}(i_t, j_{t+k})$ between nodes i_t and j_{t+k} is the length of the time-respecting shortest-path connecting i_t to j_{t+k} in $\widetilde{G}$. Two brain regions can have different time-respecting distances when active within distinct *CC*s. Note that the time-respecting distance d_{tr} of two brain regions that participate in the same *CC* is lower-bounded by the static distance d_s of the two regions, i.e., by the length of the shortest path connecting the two regions in the static structural graph *G*.

Defining a feature space for connected components and clustering

Each *CC* of $\widetilde{G}$ collects the functional activation of distinct brain regions, which can be represented as a spatial activation map. Particularly, we define a spatial activation map as a vector $\bar{x}$ of length *N*, with *N* number of brain regions. Each entry x_i of $\bar{x} = [x_1, x_2, \ldots, x_N]$ is the number of time points region i is active within the component, normalized by the vector l2-norm $|\bar{x}| = \sqrt{\sum_{i=1}^{N} |x_i|^2}$ (Fig. 2b). We can

study characteristic spatial maps of activation, by clustering the activation maps associated with multiple *CC*s. The normalization of the feature vectors by their l2-norm helps clustering together *CC*s with similar spatial activation maps but different temporal spans.

Motifs of functional activity propagation

In order to characterize the spatio-temporal behavior of the connected components, we introduce the concepts of temporal envelope and activity-propagation map (Fig. 2c).

We define the temporal envelope of a connected component of $\widetilde{G}$ as a curve that represents the number of brain regions active within each layer of the *CC*, normalized by the total number of brain regions enrolled in the *CC*. The temporal envelope of a *CC* quantifies the extent of its spatial recruitment over time. Temporal envelopes representing *CC*s with the same temporal span can be easily compared.

We define the activity-propagation map of a connected component of $\widetilde{G}$ as a vector $\bar{y}$ of length *N*, with *N* number of brain regions. Each entry y_i of the vector $\bar{y} = [y_1, y_2, \ldots, y_N]$ represents the average over the set of normalized time points at which region *i* has been active within the *CC*. The normalized time is computed by re-scaling the temporal axis of the individual *CC*s to a continuous interval [0,1], where 0 corresponds to the first time point of the *CC* and 1 corresponds to the last time point of the *CC*. The temporal normalization allows comparing the activity-propagation maps of connected components with different temporal spans.

Experimental data

Subject cohort and MRI acquisitions

We investigated the brain structural connectivity and functional dynamics of 71 healthy subjects (aged 28.8 ± 9.1 yo, 43 males). Each subject underwent an MRI session on a 3 T scanner (Magnetom TrioTim, Magnetom Prisma, Siemens Medical Solutions), equipped with a 32-channel head coil. The MRI session included (1) a magnetization-prepared rapid acquisition gradient echo (MPRAGE) sequence (1x1×1.2 mm resolution; 240x257×160 voxels; TR, TE, TI = 2300, 2.98, 900 ms); (2) a diffusion spectrum imaging (DSI) sequence (2.2×2.2×3 mm resolution; 96x96×34 voxels; TR, TE = 6100, 144 ms; q4half acquisition scheme with maximum b-value 8000 s/mm^2, one b0 volume); (3) a 9-min gradient echo planar imaging (EPI) sequence sensitive to blood-oxygen-level dependent BOLD contrast (3.3×3.3×3.3 mm resolution; 64x58×32 voxels; 280 time points; TR, TE = 1920, 3 ms). During the fMRI acquisitions, subjects were lying in the scanner with eyes open, resting but awake and cognitively alert. Additional details on the MRI acquisitions are reported in the Inline supplementary Methods, *MRI acquisition reporting*. The b-table for the DSI acquisition is reported in the Inline supplementary Table S2. Informed written consent in accordance with our institutional guidelines (protocol approved by the Ethic Committee of Clinical Research of the Faculty of Biology and Medicine, University of Lausanne, Switzerland) was obtained for all the subjects.

MRI data processing

The MPRAGE volume of each subject was segmented into white matter, grey matter and cerebrospinal fluid compartments using FreeSurfer software (Dale et al., 1999), version 5.0.0. The cortical volumes were segmented into *N=448* regions of interest as defined in Cammoun et al. (2012) (Inline supplementary Fig S3). Subcortical structures and the brain stem were excluded from further analyses. DSI data were reconstructed according to Wedeen and colleagues (Wedeen et al., 2005), thus estimating an orientation distribution function (ODF) in each voxel. Up to three main fiber orientations were identified in each voxel as the largest maxima of the ODF (DiffusionToolkit software, http://www.trackvis.org/dtk). Deterministic streamline tractography (Jones, 2008) was performed initiating 32 streamline propagations *per* white matter voxel and *per* fiber orientation. The MPRAGE and the brain parcellation were linearly registered to the subject diffusion space (b0) using a boundary-based cost function (FreeSurfer software, Greve and Fischl, 2009). Morphological and diffusion data were used to construct subject-wise structural connectivity graphs. Thereafter, a group-representative structural graph *G=(V,E)* was estimated by combining the structural graphs of the 71 subjects. Two regions *i, j* were connected in *G* if at least one streamline connected regions *i* and *j*, in at least 50% of the subjects (see Inline supplementary Fig. S4). The resulting group-representative graph had density equal to 3.3% and diameter equal to 7 hops.

fMRI data were processed as follows. For each subject, the first four fMRI volumes were discarded to allow signal stabilization. The remaining *T*=276 volumes were motion-corrected by applying a rigid body co-registration using FSL software (Jenkinson et al., 2002). Scrubbing parameters were computed on co-registered volumes and before further processing steps according to Power et al. (2012), Power et al. (2014). The *FD* and *DV* time series of the 71 subjects are reported in Inline supplementary Fig. S5. Three out of 71 subjects were excluded from further analyses because presenting more than 10% time points with extreme *FD* or *DV* values (FD > 0.5 mm, DV > 20, Power et al., 2014). Voxel-wise signals were linearly detrended and corrected for physiological confounds and artifacts by regressing the average white matter and cerebrospinal fluid signals and the six motion signals (three translations and three rotations). Finally, the fMRI volumes were spatially denoised using total variation regularization, which promotes piece-wise spatial smoothness (Michel et al., 2011), and band-pass filtered (0.01–0.1 Hz) using a Hamming windowed sinc FIR filter. The MPRAGE and the brain parcellation were linearly registered to the subject mean fMRI volume (FSL software, Jenkinson et al., 2012) in order to extract representative ROI-wise time series. The average fMRI time series associated with each cortical region were z-scored and collected in the matrices S_s^z, with $s \in [1,2, \ldots, 68]$ subject index. All the MRI processing steps were performed in subject native space using the Connectome Mapper Toolkit (Daducci et al., 2012) and dedicated Matlab and Python code.

Spatio-temporal connectomics

The z-score normalized time series S_s^z were converted to binary point-processes P_s by applying a thresholding with τ=2 standard deviations. We have chosen the threshold value by analyzing the average properties of the P_s matrices and of the resulting multilayer graphs over different threshold values (see Inline supplementary Methods, *Parameter Selection* and Inline supplementary Fig S6). A spatio-temporal connectome was constructed for each subject by merging functional (P_s) and structural (G) information in a single multilayer graph $\widetilde{G}_s$. Each spatio-temporal connectome counted *T*=276 layers corresponding to as many fMRI time points; each layer counted *N*=448 nodes corresponding to as many cortical regions, for a total of 123'648 nodes.

Transient networks of spatio-temporal connectivity

The weakly connected components of the subject-level spatio-temporal connectomes were extracted and further characterized. The *CC* spatial activation maps were clustered using a *k*-means algorithm, with number of clusters *k*=12. We chose an unsupervised clustering algorithm as spatial activation groups are not known *a priori*. We set the value of *k* by considering metrics of clustering quality and consistency across the 68 subjects (see Inline supplementary Methods, *Parameter Selection* and Inline supplementary Fig S7). The k-means clustering was repeated 100 times with random initialization, and the solution with the minimum inertia was selected. The cluster centroids represent average spatial patterns of activation between anatomically connected brain regions and were dubbed 'structure-function activation templates' (*sfAT*s). The *sfAT*s were compared with publicly available resting-state and task-based functional connectivity

networks (Laird et al., 2011; Yeo et al., 2011) by means of the Dice coefficient (see Inline supplementary Methods, *Structure-function activation templates and reference networks*). The temporal envelopes and the activity-propagation maps of the *CC*s were as well investigated. Average activity-propagation maps were computed for all the connected components classified in each *k*-means cluster to highlight waves of activity propagation characteristic of different brain functional systems.

Results

Functional co-activations and framework hypotheses

Synchronization of high-amplitude fMRI events

We investigated the functional dynamics of 68 healthy subjects (3 out of 71 subjects were discarded because of fMRI motion). For a point-process threshold τ=2 standard deviations, the total number of high-amplitude events for a single subject was 3'171 ± 228 (average and standard deviation values from 68 subjects) over a recording time of 276 time points (approximately 9 min). Therefore single brain regions were active 7 ± 3 time points on average, corresponding to 2.5 ± 1% of the overall recording time. These results are consistent with other point-process analyses of resting-state recordings (Liu and Duyn, 2013; Tagliazucchi et al., 2016). The regions with the longest activation time were concentrated over the primary sensory cortices, including somatosensory, visual and auditory areas (Fig. 5a). Somehow consistently, previous literature shows that these regions demonstrate highly stable functional connectivity over long resting-state recordings (Gonzalez-Castillo et al., 2014; Shen et al., 2015).

When considering functional co-activations between pairs of brain regions, the total number of co-activations for a single subject was 54'016 ± 11'871. The overall number of co-activations was significantly higher than what expected by chance (independently phase-randomized time series, 13'581 ± 50 co-activations, two-sided Wilcoxon rank sum test $p < 10^{-12}$) (Fig. 3c). Moreover, the number of co-activations was significantly higher than what expected for a multivariate process with preserved autocorrelation and cross-correlation properties (uniformly phase-randomized time series, 41'194 ± 7'490 co-activations, $p < 10^{-6}$) (Fig. 3c). The number of co-activations between pairwise orthogonalized fMRI times series was 19'986 ± 8'000, significantly higher than what expected by chance (independently phase-randomized time series, $p < 10^{-9}$) (Fig. 3c). These results indicates that the co-activation patterns inferred from a fMRI point-process analysis and included in the spatio-temporal connectomes are functionally meaningful and cannot be explained by time-average bivariate relationships only.

Functional interactions and anatomical connectivity

Previous studies have shown that a significant time-average functional correlation can exist between brain regions with no direct structural connection (Goñi et al., 2014; Honey et al., 2009). In the present study we connected two nodes in the multilayer graphs only if a direct anatomical tract connects them. We now ask if reproducible time-resolved functional relationships exist between brain regions with no direct structural connection. We found that co-activations of anatomically connected regions occur, on average, twelve times more often than co-activations of non-connected regions (151.1 ± 96.4 against 12.8 ± 11.7 times over the 68 subjects; Wilcoxon rank sum test $p < 10^{-10}$) (Fig. 4). This strong unbalance suggests that, on the temporal scale of seconds, the large majority of reproducible functional interactions involves brain regions with a direct structural connection. At this short temporal-scale, interactions between brain regions with no direct structural connection are mostly non-reproducible and possibly related to noise.

The recurrence of pairwise interactions between anatomically connected regions can be represented in the form of an asymmetric

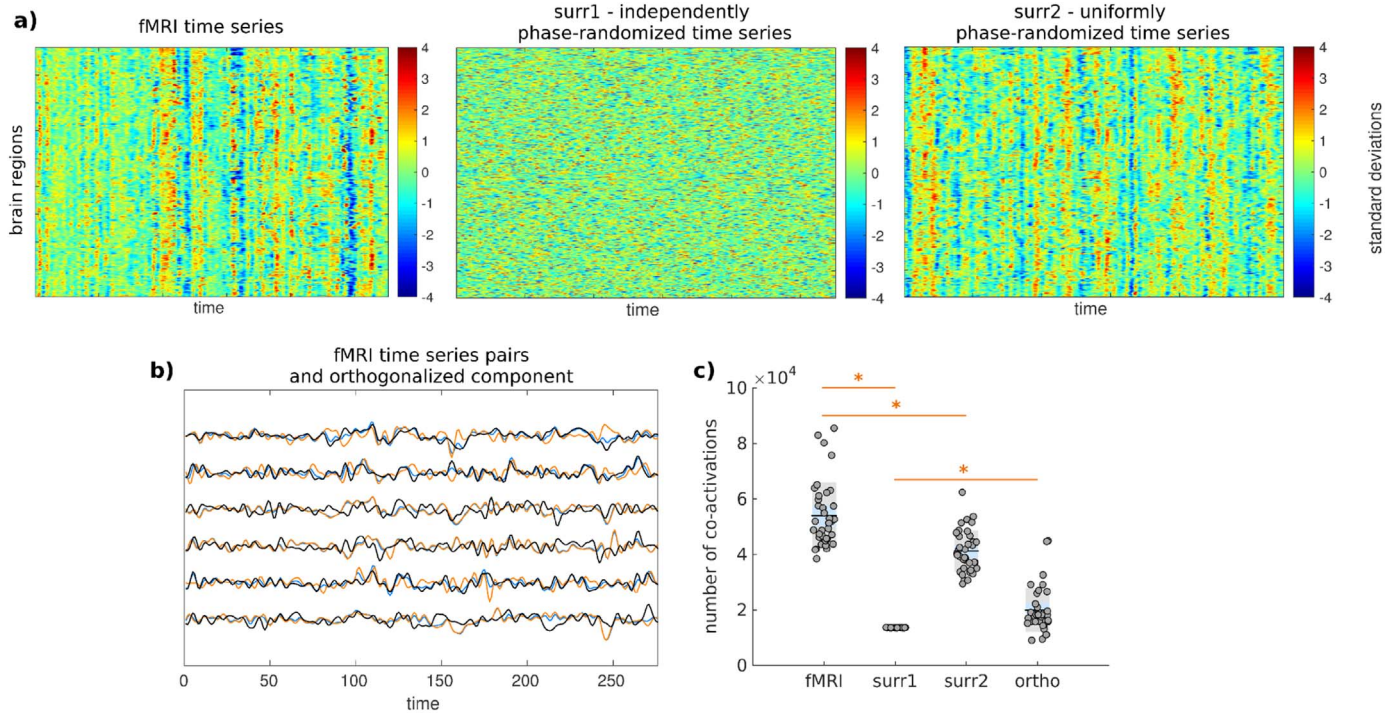

Fig. 3. Spatio-temporal framework hypotheses and surrogate data. (a) z-score fMRI time series and relative surrogate data (independently phase-randomized time series and uniformly phase-randomized time series) for an example subject. The time series matrices have size 448 brain regions X 276 time points. (b) Examples of pairwise randomized time series for the same subject. The orange lines represent the orthogonal component of a first time series (blue lines) with respect to a second time series (black lines). (c) Number of functional co-activations detected in a complete 9-min fMRI recording ('fMRI' boxplot) and in relative surrogate data ('surr1': independently phase-randomized time series; 'surr2': uniformly phase-randomized time series; 'ortho': pairwise orthogonalized time series). Each circle in the boxplot represents the number of co-activations detected in a single subject. The average number of co-activations over 100 repetitions is reported for datasets 'surr1' and 'surr2'. Asterisks indicate statistically significant differences. 37 subjects were considered for this analysis.

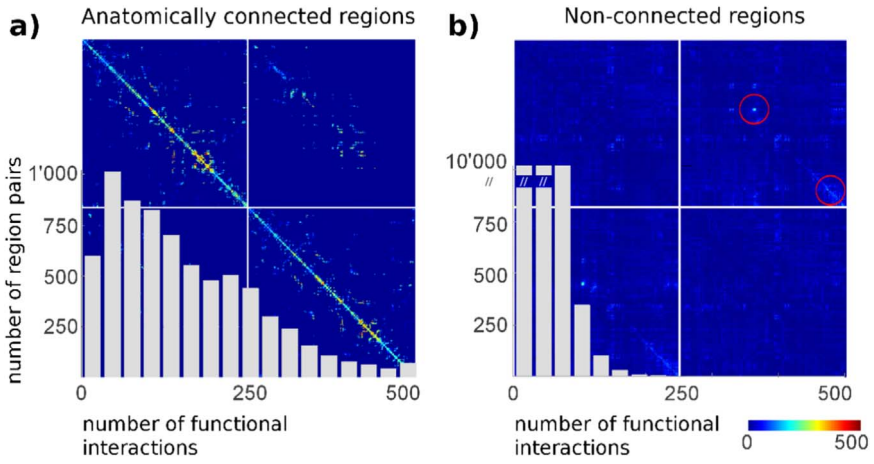

Fig. 4. Reproducibility of functional co-activations between anatomically connected and unconnected region pairs. The two matrices represent the recurrences (over the 68-subject recordings) of functional co-activations between pairs of brain regions (a) connected and (b) non-connected by a direct anatomical link. The first and forth matrix quadrants refer to the intra-hemispheric functional relationships; the second and third quadrants to the inter-hemispheric ones. The histograms of the non-zero entries of the recurrence matrices are represented in gray. The red circles in (b) highlight the functional relationship between the bilateral auditory cortices, and the lateral postcentral gyri.

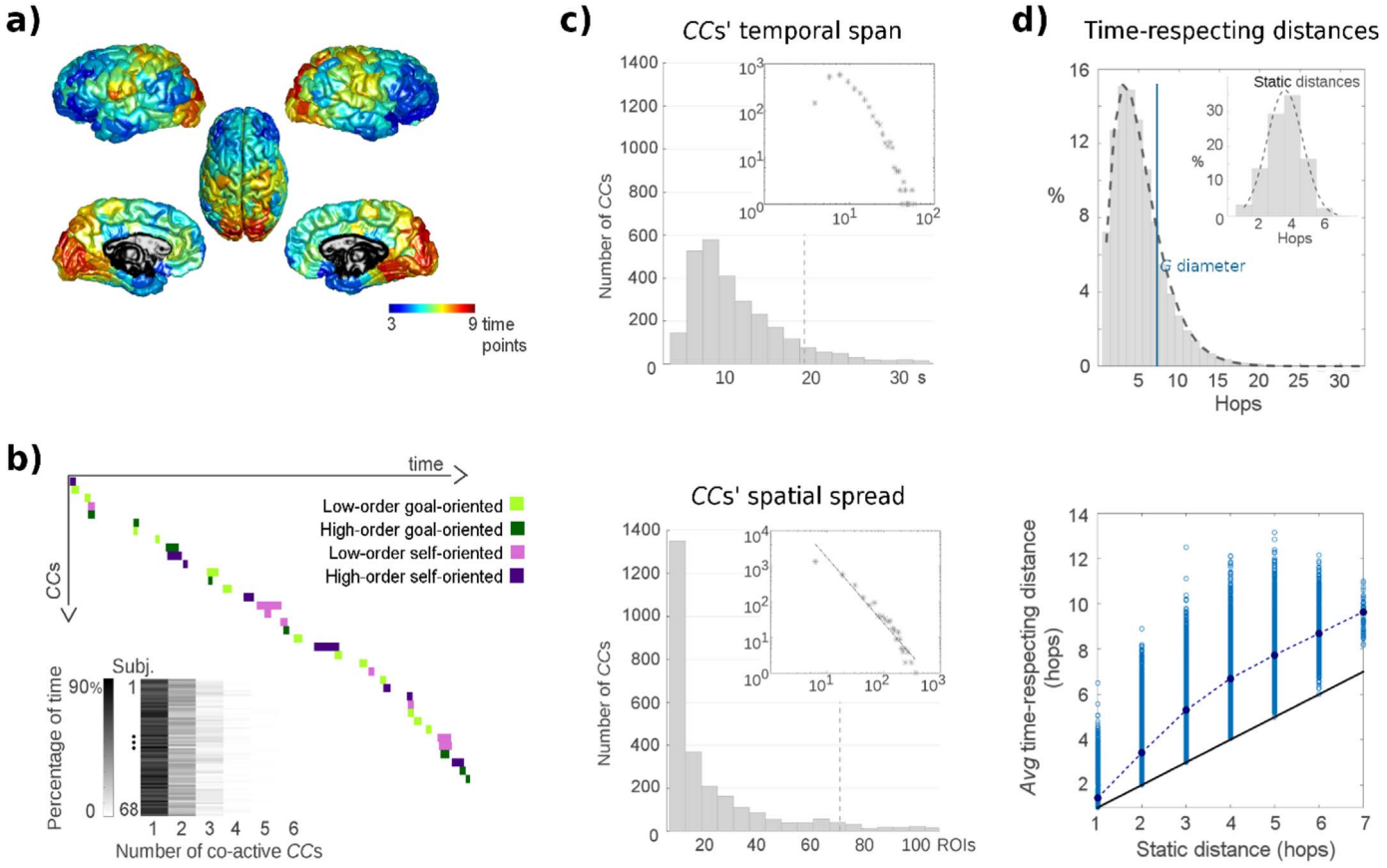

Fig. 5. Local activations and connected components' characterization. (a) Brain surface map representing the average duration of local activations extracted from fMRI data and point-process analysis (9-minute recordings with 276 time points; average over 68 subjects). Areas of longest activation cover the primary sensory cortices including somatosensory, visual and auditory regions. (b) Connected components and temporal overlap. The colored plot outlines a typical *CC*s sequence (data from one example subject): the blocks represent the temporal span of the single *CC*s and are color-coded according to their classification into low- and high-level goal-oriented and self-oriented functional systems (see Fig. 6). The *CC*s partially overlap in time: the grey-level plot shows the percentage of time each subject (*y*-axis, 1st to 68th subject) spends having multiple (up to 6, *x*-axis) co-active *CC*s. (c) Distributions of the temporal span (seconds) and spatial spread (number of anatomical region of interests (ROIs)) of the 2'561 *CC*s extracted from our cohort. The dot-lines indicate the distributions' 90th-percentile (19.2 s and 71 ROIs). Inset plots: representation in log-log scale of the two distributions. The dashed line in the spatial spread log-log plot represents the least-squares power-law fit with slope α=−1.8. (d) Distribution of the time-respecting distances and static distances. The histogram of the time-respecting distances is heavy tailed and was fitted with a gamma distribution (k=2.70, θ=1.91); the vertical line represents the diameter of the static structural graph (7 hops). The histogram of the static distances was fitted with a normal distribution (μ=3.54, σ=1.10). Lower plot: Average time-respecting distances between pairs of brain regions and corresponding static distance. The black line represents the identity line; the dashed curve links the median values of the time-respecting distances associated with each static distance.

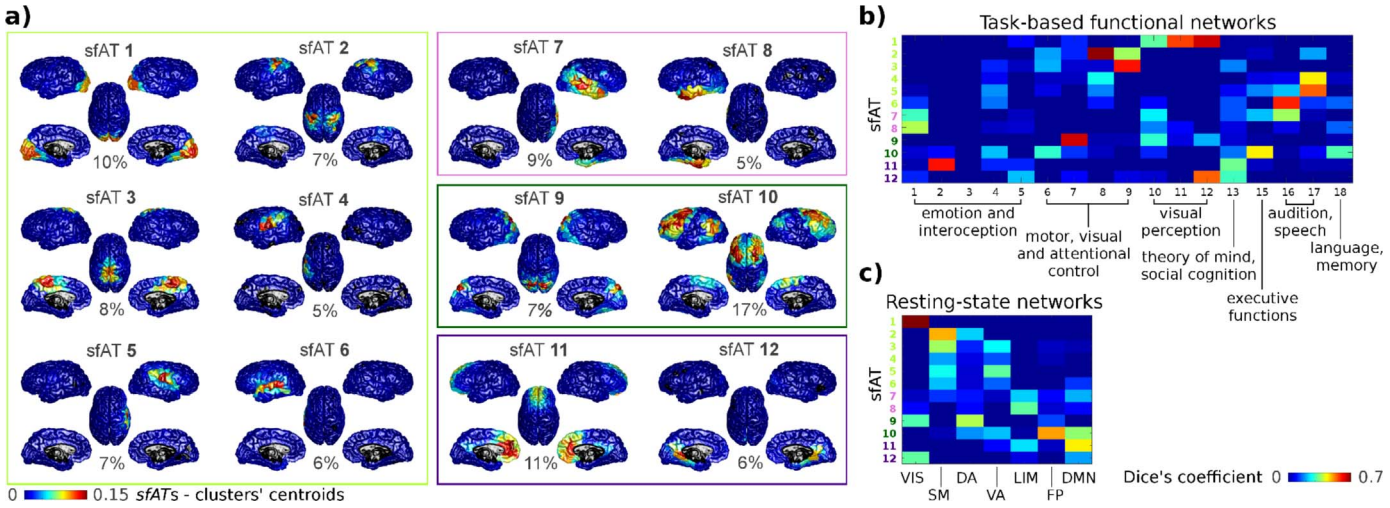

Fig. 6. Structure-function activation templates (*sfATs*). (a) Brain-surface plots picturing the centroids of the 12 *CC* clusters (*sfATs*). The color coding represents the average, normalized temporal duration of the local activations over the *CCs* classified in the same cluster. The percentages of the total 2'561 *CCs* classified in each cluster are reported. The *sfATs* are grouped according to their qualitative classification into goal-oriented (green) and self-oriented (violet) systems, differentiating low-order (light colors) and high-order (dark colors) functions. (b) Overlap between the 12 *sfATs* and the 17 Intrinsic Connectivity Networks -*ICNs*- (task-based functional networks) identified by Laird and colleagues (Laird et al., 2011). *ICNs* 14, 19 and 20 were not shown in this plot because they corresponds to cerebellar regions (not included in our investigation) or fMRI artifacts (Laird et al., 2011). (c) Overlap between the 12 *sfATs* and the 7 RSNs identified by Yeo et al. (2011). 'VIS' visual, 'SN' sensorimotor, 'DA' dorsal attention, 'VA' ventral attention, 'LIM' limbic, 'FP' frontoparietal, 'DMN' default mode network. The overlap between functional maps was evaluated with the Dice's coefficient.

connectivity matrix (Fig. 4a), that has the same binary structure of the graph *G*. The connection weights map the frequency of directed anatomical tracts recruitment within the transient networks of spatio-temporal connectivity (*CCs*). Similarly, the count of pairwise interactions between regions with no direct structural link can be represented in the form of a recurrence matrix (Fig. 4b) with globally low values but non-random structure, indicating that some anatomically non-connected regions (e.g., the bilateral auditory cortices or the lateral postcentral gyri, circled in red in Fig. 4b) are recurrently engaged in distinct but temporally co-occurring *CCs*. On one hand, these systems could be brought to temporal synchronization through external stimuli, like a sound. On the other hand, the structural connectivity graph could be deficient in fibers that are difficult to track, such as the commissural fibers (Thomas et al., 2014). Furthermore time-resolved functional connectivity may occur through multi-step structural connections not included in the spatio-temporal connectomes, which is possible given the limited sampling rate of the investigated fMRI recordings and the intrinsic limitations of dMRI tractography and structural connectome mapping. For instance the left and right auditory cortices, that form two distinct *sfATs*, receive common neural inputs from both hears *via* the pons and thalamus, which are not included in our connectivity model.

Transient networks of spatio-temporal connectivity

We investigated the spatio-temporal connectomes of 68 healthy subjects. The spatio-temporal connectomes could be described as dense sequences of transient spatio-temporal networks (*CCs*) partially overlapping in time. The average number of *CCs per* subject was 38 ± 8, for a total of 2'561 *CCs*. 126 *CCs* were excluded because overlapping time points associated with motion (extreme *FD* or *DV* values, see Inline supplementary Fig. S5) and are not considered here. The average temporal span of the single *CCs* was 11.0 ± 6.3 s (90% of the *CCs* lasted less than 19.2 s); the spatial spread of the *CCs* was 27 ± 35 regions (90% of the *CCs* included less than 67 regions). The distributions of the temporal and spatial *CC* spreads were heavy-tailed (power-law fit with exponent α=−1.8), with a minority of *CCs* presenting a broad spatio-temporal extension (Fig. 5b). Despite the high temporal and spatial sparsity of the structural and functional data (single brain regions were active 2.5 ± 1% of the overall recording time; the density of the structural graph was 3.3%), the *CCs* of the spatio-temporal connectomes were active 293.4 ± 53.4 s *per* subject corresponding to 55.4% of the overall recording time, thus indicating that the resting-state dynamics are highly spatio-temporally organized. We note that resting-state activations co-occurring in time but involving brain regions not directly connected through white-matter tracts were assigned to distinct *CCs* (Inline supplementary Fig S2). The temporal overlap between *CCs* was on average 33% of the overall *CCs*' activation time (Fig. 5c).

The transient spatio-temporal networks select viable white matter pathways of functional activity propagation (or functional paths). In order to investigate the length distribution of these paths we evaluated the time-respecting distances between all pairs of brain regions participating in single *CCs*. The distribution of the functional paths length was heavy tailed (gamma distribution fitting with k=2.70, θ=1.91), with 19% of the values exceeding the diameter of the structural graph *G* (median and maximum values 5 and 33 hops, Fig. 5d). The relationship between functional paths length and static shortest paths length (static distances computed on the structural graph *G*) was monotonic but not linear (Fig. 5d). Functional paths were on average 70 ± 35% longer than the static ones and their length predicted static functional connectivity values with higher accuracy than static shortest path length. Particularly, the linear correlation between time-respecting distances and time-average functional correlations (evaluated on an independent dataset) was r=−0.486 ($p < 10^{-15}$) and outmatched the predictive capacity of the static distances (r=−0.311, $p < 10^{-15}$) (see Inline supplementary Methods, *Static functional connectivity prediction* and Inline supplementary Fig S8). This result constitutes a good sanity check of our approach and is expected since the time-respecting paths encode functional information which is not encoded in the static shortest paths.

Taken together, these findings suggest that the propagation of dynamic processes on the structural connectome could follow polysynaptic pathways significantly different from the static shortest paths.

Reproducible patterns of spatio-temporal connectivity

In order to retrieve reproducible patterns of spatio-temporal connectivity, recurrent across fMRI recordings and multiple subjects, we classified the overall 2'561 *CCs* into twelve clusters. The cluster

centroids are shown in Fig. 6a and are interpreted as structure-function activation templates (*sfAT*) that represent the average spatial patterns of transient functional synchronization among anatomically connected brain regions. The *sfAT*s can be grouped according to their concordance with known functional systems, and are compared with publicly available task-based (ICNs) and resting-state (RSNs) functional networks using the Dice's coefficient (Fig. 6b, c). The first 6 *sfAT*s relate to low-order sensorimotor tasks including visual and visuospatial tasks, audition and speech (see the overlap with the visual and sensorimotor RSNs, Fig. 6c). The *sfAT* 1 includes the primary and secondary visual cortices, with sustained activation localized in the cuneus, pericalcarine sulci and lingual gyri, and it extends toward the fusiform and the lateral occipito-temporal junctions. The *sfAT*s 2 and 3 encompass the pericentral sensorimotor areas, covering the precentral and postcentral gyri and the paracentral lobule (ICNs 8 and 9, Fig. 6b). The *sfAT*s 4 and 5 are symmetric with respect to the brain medial line. They include the lateral extremities of the pre- and post-central gyri and are associated with task-based networks of sensorimotor functions for the mouth (ICN 17). Taken together, the *sfAT*s 2 to 5 encompass the sensorimotor cortices of the superior limbs (*sfAT* 2), inferior limbs (*sfAT* 3) and face (*sfAT*s 4 and 5). The *sfAT*s 6 and 7 contain, respectively, the left and right auditory areas, localized mainly over the superior and transverse temporal gyri and well overlapping task-based networks related to audition and speech (ICN 16). On the right side, the *sfAT* 7 extends toward the medial-temporal and limbic association cortices, related to emotional and interoceptive processing (ICN 1). On the left side, the auditory and limbic areas constitute two separate clusters (*sfAT*s 6 and 8). Taken together, the *sfAT*s 7 and 8 can be associated with low-order emotional and self-oriented tasks. The *sfAT* 9 covers large part of the dorsal attention network (see overlap with Yeo RSNs), including the occipital, superior and inferior parietal areas. It is involved in top-down attentional control (ICN 7) and visual association tasks (ICN 10). The *sfAT* 10 covers bilateral fronto-parietal regions and corresponds to the executive network (cognitive processing and working memory tasks, ICNs 15 and 18, fronto-parietal RSN). Lastly, sfAT 11 and 12 relate to high-order self-oriented processes. The *sfAT* 11 involves dorso-medial and ventro-medial prefrontal cortices and extends to the anterior and posterior cingulate. The *sfAT* 12 includes the most ventral parts of the precuneus and posterior cingulate cortex, and extends towards the lingual and parahippocampal gyri. Those regions are known to be involved in emotional processing, social cognition and theory of mind (overlap with ICN 2 and 13).

On one side we can observe that the *sfAT*s are behaviorally meaningful and relate to the brain's main functional systems, as indicated by the overlap with task-based networks (note the sparsity of the Dice's coefficient matrix in Fig. 6b) (Laird et al., 2011). On the other side, the classical RSNs (Yeo et al., 2011; Damoiseaux et al., 2006; Fox et al., 2005) appear to be split among multiple *sfAT*s. For example, the sensorimotor RSN and the default mode network (DMN) are shared among multiple low-order and high-order *sfAT*s (Fig. 6c), confirming previous literature (Karahanoğlu and Van De Ville, 2015; Betzel et al., 2016). Finally, it is worth noting that the *CC*s classified in each cluster can significantly diverge from the centroid map (i.e., from the *sfAT*). Indeed the *CC*s are characterized by highly variable temporal and spatial span (Fig. 5c and Inline supplementary Table S1) and can engage different sets of brain regions and anatomical connections (as exemplified in the *Inline supplementary Video S1*).

Supplementary material related to this article can be found online at http://dx.doi.org/%2010.1016/j.neuroimage.2017.04.015.

Split resting-state networks: Probing the DMN

The DMN is a well-characterized RSN (Raichle 2015), but it does not appear as a distinct *sfAT* (Fig. 7) and deserves further attention. We hypothesize that, in a spatio-temporal connectome analysis, the DMN is split among different *sfAT*s, and that its constituent regions interact in a way that is not constant over time. In order to probe this hypothesis, we first derived a DMN map by means of a time-average seed-based correlation analysis from the bilateral precunei (Fig. 7a, see Inline supplementary Methods, *DMN Analysis*). As quantified by a

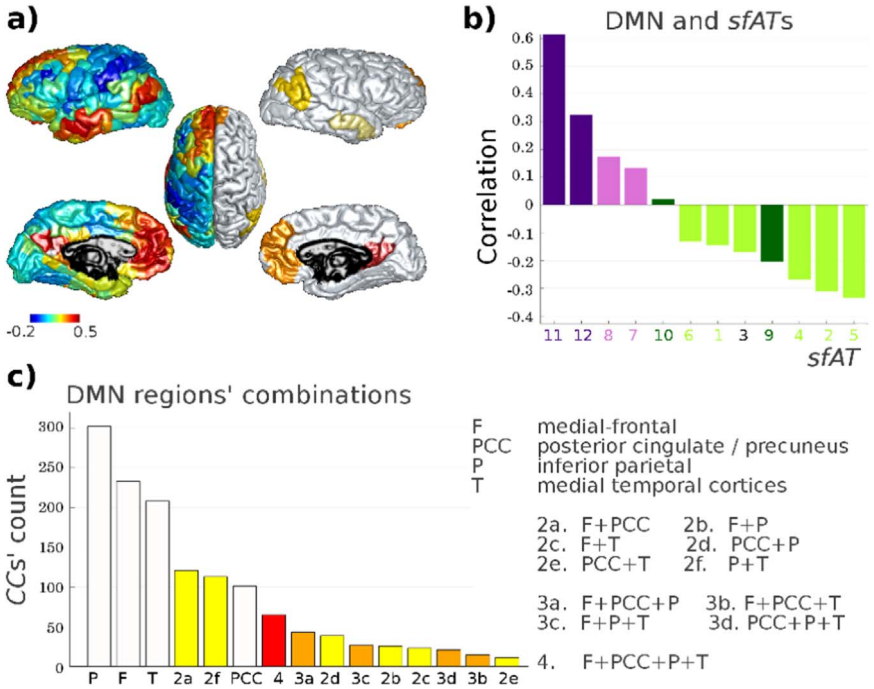

Fig. 7. Dynamic behavior of the DMN. (a) Left hemisphere: DMN average correlation map from precuneus seed region (in gray). Right hemisphere: medial frontal (orange, F), posterior cingulate / precuneus (red, PCC), inferior parietal (gold, P) and middle temporal (light yellow, T) DMN regions. (b) Similarity between the twelve *sfAT*s and the DMN map, as quantified by Pearson's linear correlation. The color-coding represents emotional and self-oriented (violet) *vs* external and goal-oriented functional templates (light colors: low-order, dark colors: high-order system, as in Fig. 5). (c) Recurrence of different DMN regions' combinations in single *CC*s. The bar color indicates the number of DMN regions included in each combination (from white to red: 1 to 4 DMN regions). The different DMN regions' combinations are not equiprobable.

spatial correlation measure, the DMN overlaps mainly with high-order (*sfAT* 11 and 12, related to theory of mind) and low-order (*sfAT*s 8 and 9, related to emotions' processing) self-oriented circuits, whereas its spatial pattern excludes goal-oriented activation templates (Fig. 7b). We then considered the *CC*s of the spatio-temporal connectomes including at least one DMN region. The DMN can be decomposed into four bilateral regions (Fig. 7a): medial-frontal areas (F), posterior cingulate cortices / precuneus (PCC), inferior parietal cortices (P) and middle temporal cortices (T). The DMN regions were highly represented in the *CC*s: 52.5% of the total 2'561 *CC*s contained at least one DMN region spanning 61.7% of the overall *CC*s' activation time; 19.7% of the total 2'561 *CC*s contained at least two DMN regions spanning 29.5% of the overall *CC*s' activation time. The *CC*s including DMN regions did not always engage all the four F/PCC/P/T areas. Instead, the four DMN regions were rather independently or synchronously active, with preferential patterns of combined functional engagement. Fig. 7c shows the recurrence of the *CC*s including all the 15 possible combinations of DMN regions (taken 1, 2, 3 or 4 at a time) over recording time and subjects. The most probable combinations were: the independent activation of the four DMN regions (particularly frontal and parietal areas), followed by fronto-posterior cingulate (F +PCC) and parieto-temporal (P+T) activations, and the complete four-region DMN activation (F+PCC+P+T). Other combinations were less frequent.

Motifs of functional activity propagation

We asked if the functional activity propagation within the *CC*s forms particular spatio-temporal motifs. To this end, we grouped the 2'561 *CC*s on the basis of their temporal duration and investigated their temporal envelopes. We found that, independently of the overall duration, a *CC* activity starts from a small set of brain areas (10% to 40% of the regions recruited in the single *CC*s), propagates to a large set (40% to 80% of the *CC*'s regions) and then vanishes toward a small set (10% to 40% of the *CC*'s regions) of brain areas, following an expanding-shrinking motifs (Fig. 8a).

To further investigate the spatio-temporal propagation patterns for the distinct brain functional systems, we computed the average activity-propagation map for each *sfAT* cluster. The average propagation maps demonstrate non-random spatial patterns (Fig. 8b). In the visual system (*sfAT*s 1, 2) the functional activity propagates from the fusiform cortices to the cunei and superior parietal areas. In the sensorimotor circuits, the functional activity propagates from the lateral pericentral cortices and cingulate gyri to the superior parietal lobules (*sfAT*s 3), and from the lateral extremities of the pre- and post-central gyri toward higher-order somato-sensory regions as the supra-marginal and insular cortices (*sfAT*s 5, 6).

Discussion

In this work, we integrated brain anatomical connectivity and narrow-band (0.01–0.1 Hz) functional activity (as derived from diffusion and functional MRI) into a single multilayer graph (Kivelä et al., 2014), a convenient mathematical framework for the analysis of fMRI dynamics (Bassett et al., 2013; Braun et al., 2015). Particularly, we explicitly included in the graph the anatomical connectivity information. This enables the investigation of structure-function interplays and of dynamic routing of functional interactions on the structural connectome. The framework captures transient spatio-temporal networks (i.e., *CC*s) (Kivelä et al., 2014; Nicosia et al., 2012), characterized by specific spatial configurations and temporal dynamics.

We studied the spatio-temporal connectomes of a group of 68 healthy subjects and investigated the resulting 2'561 connected components (3 out of 71 subjects were excluded because of excessive motion in the fMRI recordings). For each subject, the sequence of *CC*s can be clearly followed, is not trivially cyclic and individual *CC*s can overlap in time. The distributions of the duration and spatial spread of the *CC*s are heavy-tailed and approximate power-law functions. This observation adds to previous reports that suggest that the brain works in a self-organized critical state, across different frequency bands of activity (Kitzbichler et al., 2009; Tagliazucchi et al., 2012).

The clustering of the *CC*s reveals well-known circuits relating to classic RSNs and behaviorally meaningful functional network (Fig. 6), thus suggesting that the spatio-temporal connectivity is a relevant phenomenon in the self-organization of functional systems. However, the spatial and temporal heterogeneity of the *CC*s (Fig. 5, *Inline supplementary Video S1*) indicates that the resting-state transient networks are more complex than the time-average RSNs. This complexity could reflect a dynamic and flexible communication-rerouting in response to a large variety of external and internal inputs, such as

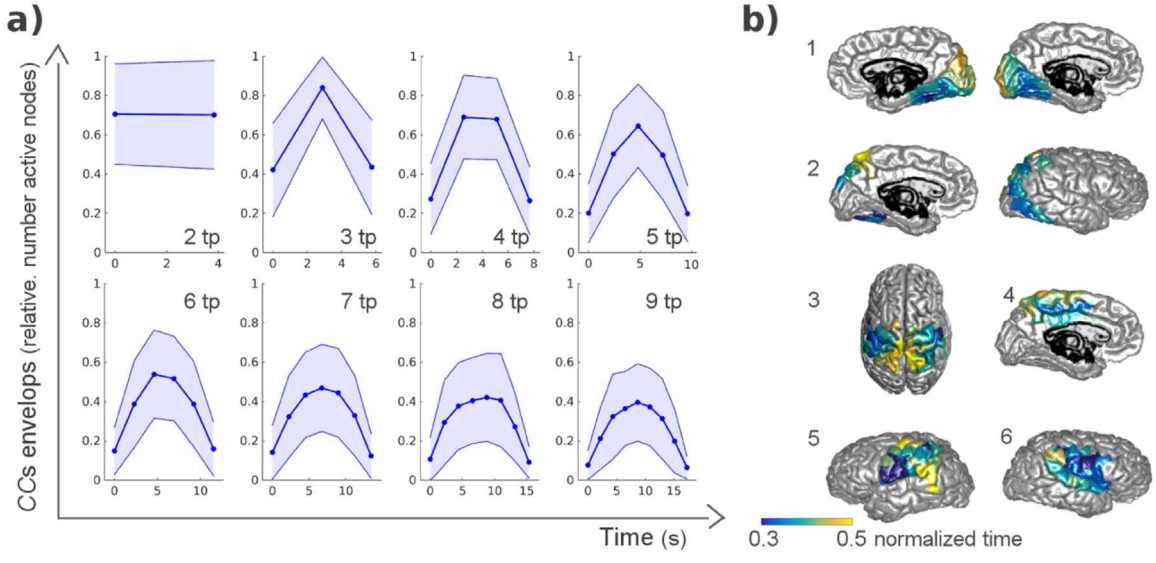

Fig. 8. Temporal envelopes and activity-propagation maps. (a) Examples of temporal envelopes of *CC*s with different durations (2, to 9 time points, corresponding to 3.8 to 17.3 s). The mid-lines and the colored areas represent the percentage of the *CC*'s active regions over time (average ± one standard deviation). (b) Examples of average activity-propagation maps represented on the cortical surface. The maps illustrate the timing of activity propagation and have been obtained by avaraging the temporal patterns of all the Ccs classified in the clusters *sfAT* 1, 2, 3, 4, 5 and 6. The color-coding indicates the average first activation time point of the different brain regions within the *CC*s of the spatio-temporal connectomes(time scale normalized to the range [0,1]).

selective attention or sensory-stimuli processing (Bassett et al., 2013; Betzel et al., 2016; Braun et al., 2015), and cognitive requirements (Bassett et al., 2011). The case of the default mode network (DMN) is a prominent example of dynamical coupling. Others before us have shown that the DMN breaks over time into heterogeneous patterns (Hutchison et al., 2013; Karahanoğlu and Van De Ville, 2015; Raichle 2015), and that its component regions frequently switch among different functional communities (Betzel et al., 2016; Zalesky et al., 2014). Our data reveal that the DMN regions interact in a way that is not constant over time and transiently synchronize in configurations that are heterogeneous and not equiprobable.

The connected components present characteristic spatio-temporal patterns of functional activity propagation. Typically, the functional activity starts within a focal area, then spreads by recruiting an increasing number of brain regions, reaches a peak of massive activation and finally fades out in some specific location. Within the different functional systems, some brain areas appear to be recruited on average earlier than other in a resting-state condition. For example, the fusiform-cortex activation often precedes the cuneus and superior parietal activations in the visual circuit; the activation of the lateral pericentral cortices precedes the activation of supramarginal regions in the ventral attention network. These findings are in line with previous reports that describe 'waves' of high signal-intensity propagation (Majeed et al., 2011) and 'lag threads' including 'early' and 'late' nodes' activity in fMRI recordings (Mitra et al., 2015), and they extend such reports by explicitly linking the propagated activity and the anatomical substrate. Indeed, the propagation of functional activity selects sets of viable structural pathways for functional communication. Among these, the time-respecting shortest paths of the spatio-temporal transient networks appear as viable and convenient structural routings for communication. We found that the time-respecting shortest paths were significantly longer that the static shortest paths computed on the brain structural graph (Fig. 5d, e). In line with recent studies (Avena-Koenigsberger et al., 2016; De Reus and van den Heuvel, 2014; Goñi et al., 2013), this evidence suggests that routing strategies, other than static shortest paths, might underpin communication principles of the human brain.

Although previous studies have shown that the structural connectivity shapes time-average functional correlations (Deco et al., 2011; Honey et al., 2010), the capacity of predictive and computational models to reproduce functional connectivity from structural features remains somehow limited (Goñi et al., 2014). This might result from the fact that measures of time-average functional connectivity ignores the dynamical aspects of brain activity at rest (Hansen et al., 2015). It has been suggested that high functional correlations in absence of direct anatomical links are related to indirect paths (Mišic et al., 2016) and collective effects (Adachi et al., 2012). Both direct structural connections and polysynaptic structural pathways have been associated with temporal stability of functional dynamics (Shen et al., 2015). Here we show that indeed, at the temporal resolution of fMRI recordings, the most reproducible functional interactions take place between anatomically connected brain regions but organize into larger transient networks with characteristic patterns of multi-step spatio-temporal connectivity. Moreover, due to the temporal sequentiality imposed by the framework, the frequencies of pairwise 'induced' activation of one brain region by another structurally connected regions can be estimated. The recurrences of functional interactions relate to the average (directed) usage of the structural links for the emergence of transient patterns of synchronization. With an appropriate row-wise normalization of the recurrence matrix (Fig. 4a), it is therefore possible to compute a transition matrix in the Markovian sense, where every entry encodes the probability that an active brain region activates another. In opposition to the structural connectivity matrix derived solely from dMRI data, which is symmetric, this transition matrix is asymmetric. These aspects deserve further investigation and might be relevant to the study of mechanistic brain-communication models such as diffusion (Abdelnour et al., 2014) or spreading dynamics (Mišic et al., 2015).

Our results, by characterizing transient networks of spatio-temporal connectivity, highlight patterns of activity propagation and structural-connection selection. Taking a step forward, we could interpret these transient networks as the reflection (at a macroscopic and temporally smoothed scale) of neural communication-channel selection. We dare this interpretation in light of diverse studies that identify temporal synchronization as a central mechanism for adaptive neural communication (Fries, 2015). In particular, the communication-through-coherence (CTC) hypothesis proposes that, on the microscopic scale, nervous communication and effective post-synaptic excitation are promoted by patterns of synchronization (phase-coherence) among the gamma and beta electrical oscillations of wired neuronal groups (Fries, 2005, 2015). The nervous spatio-temporal coherence on this scale would be both functional to, and a shaper of, effective communication among distinct neural units. Recent computational studies suggest that the microscale CTC mechanism could be reflected on the whole-brain macro-scale and, crucially, across different (from fast to infra-slow) time scales of brain synchronization (Deco and Kringelbach, 2016; Hansen et al., 2015). In the light of these studies, the large-scale transient networks of spatio-temporal connectivity that we observe could be the expression of the flexible and adaptive communication structure of the brain. Accordingly, the interpretability of our framework expands significantly, because we can associate spatio-temporal connectivity with the notion of information transmission and selective communication. The connected components and their time-respecting paths become transient channels of communication, thus implementing a variety of functional configurations on the top of a static anatomical substrate. The transition matrix, by quantifying the frequency of forward interactions between brain regions, conveys information fluxes. If we are speculative, the single connected components might reflect neural assemblies (Varela et al., 2001), also referred to as neuronal representations (Fries, 2015), underlying basic elements of cognitions.

Finally, it must be noted that the proposed spatio-temporal framework can be improved in several ways. The method relies on the confluence of functional dynamics and dMRI structural information. It is well known that dMRI- tractography suffers form different methodological limitations derived from both image acquisition and algorithmic factors (Jones et al., 2013), and structural connectomes contain a certain percentage of false positive and false negative connections (De Reus and van den Heuvel, 2013). Moreover, dMRI cannot recover the directionality of structural connections. These elements can bias the analysis of spatio-temporal connectivity patterns. This could for example be the case with the left and right auditory cortices that are separated in two distinct *sfAT*s in our analyses. Future work should improve the current methodological formulation by including structural connection weights (e.g., axonal fiber density or diameter) and/or connection probabilities (Daducci et al., 2016; Hinne et al., 2013). We have defined the time-resolved functional connectivity ('temporal' connectivity) using a point-process compression of the fMRI time series. Although simple and dependent on the threshold selection, this approach does not require the definition of any temporal window of analysis (Preti et al., 2017), preserves the important statistical features of resting-state signals (Tagliazucchi et al., 2016) and identifies functional patterns related to behavioral and cognitive processes (Chang et al., 2016; Chen et al., 2016). We found that at rest the frequency of co-activation patterns detected through a point-process analysis cannot be explained by the signals' time-average linear-relationships alone. This finding adds to the current debate on the stationary and non-stationary aspects of functional connectivity (Zalesky and Breakspear, 2015; Hindriks et al., 2016), and it encourages further methodological and statistical work on time-varying fMRI patterns. Within the present framework clustering algorithms other than the k-means, and tailored to complex data-distributions,

could be used to highlight further spatio-temporal hierarchies among the identified *CC*s.

It should also be mentioned that both the point-process approach and the intrinsic smoothness of the fMRI signals drastically limit the capability of temporal localization of neural events. Since the BOLD response occurs at a slower temporal scale than actual neural dynamics and since the HRF can vary across different brain regions and different subjects, it is difficult to estimate the exact timing of brain activity and lagged synchronization (Lindquist, 2008; Mitra et al., 2014). In general, mathematical approaches more sophisticated than point-process analysis can grant a more robust estimation of causal (Friston, 2011) and phase-relationships (Karahanoğlu and Van De Ville, 2015; Ponce-Alvarez et al., 2015) between local activities. Furthermore, our analyses are restricted to the infra-slow (0.01–0.1 Hz) frequency band. The investigation of multiple frequency bands, from fMRI and complementary modalities such as EEG or MEG (Chu et al., 2015; Yaesoubi et al., 2015), could extend our findings and help to clarifying causal relationships and the role of frequency encoding in the communication mechanisms that pertain to different functional systems. Indeed, the characterization of spatio-temporal connectomes, provided in this initial work, brings forward several questions. For instance, how does spatio-temporal connectivity re-organize in presence of external stimuli and task requirements, or in different conditions such as development or neuropsychiatric disorders? What is the role of time-respecting paths in driving communication-channel selection and brain plasticity? Which communication principles underlie large-scale adaptability and cognitive mechanisms? A shift from the characterization of functional dynamics to the investigation of spatio-temporal connectivity could be an instrument to expand our understanding of the flexible behavior of the brain.

Acknowledgments

This work was supported by the Swiss National Science Foundation [Grant 310030-156874]; the NCCR-Synapsy program [Grant 51AU40-125759]; and the Center of Biomedical Imaging (CIBM) of the Geneva-Lausanne Universities.

Appendix A. Supplementary material

Supplementary data associated with this article can be found in the online version at http://dx.doi.org/10.1016/j.neuroimage.2017.04.015.

References

Abdelnour, F., Voss, H.U., Raj, A., 2014. Network diffusion accurately models the relationship between structural and functional brain connectivity networks. Neuroimage 90, 335–347.
Adachi, Y., et al., 2012. Functional connectivity between anatomically unconnected areas is shaped by collective network-level effects in the macaque cortex. Cereb. Cortex 22, 1586–1592.
Allan, T.W., et al., 2015. Functional connectivity in MRI is driven by spontaneous BOLD events. PLoS One 10 (e0124577).
Allen, E.A., et al., 2012. Tracking whole-brain connectivity dynamics in the resting state. Cereb. Cortex 24, 663–676.
Avena-Koenigsberger, A., et al., 2017. Path ensembles and a tradeoff between communication efficiency and resilience in the human connectome. Brain Struct. Funct. 222 (1), 603–618.
Bassett, D., et al., 2011. Dynamic reconfiguration of human brain networks during learning. Proc. Natl. Acad. Sci. USA 108 (18), 7641–7646.
Bassett, D., et al., 2013. Task-based core-periphery organization of human brain dynamics. PLoS Comput. Biol. 9, e100317.
Benzi, K., Ricaud, B., Vandergheynst, P., 2016. Principal patterns on graphs: discovering coherent structures in datasets. IEEE T-SIPN. http://dx.doi.org/10.1109/TSIPN.2016.2524500.
Betzel, R., Fukushima, M., He, Y., Zuo, X.N., Sporns, O., 2016. Dynamic fluctuations coincide with periods of high and low modularity in resting-state functional brain networks. Neuroimage 127, 287–297.
Braun, U., et al., 2015. Dynamic reconfiguration of frontal brain networks during executive cognition in humans. Proc. Natl. Acad. Sci. USA 112, 11678–11683.
Bullmore, E., Sporns, O., 2009. Complex brain networks: graph theoretical analysis of structural and functional systems. Nat. Rev. Neurosci. 10, 186–198.
Bullmore, E., Sporns, O., 2012. The economy of brain network organization. Nat. Rev. Neurosci. 13, 336–349.
Calhoun, V.D., Miller, R., Pearlson, G., Adali, T., 2014. The chronnectome: time-varying connectivity networks as the next frontier in fMRI data discovery. Neuron 84 (2), 267–274.
Cammoun, L., et al., 2012. Mapping the human connectome at multiple scales with diffusion spectrum MRI. J Neurosci. Methods 203, 386–397.
Chang, C., et al., 2016. Tracking brain arousal fluctuations with fMRI. Proc. Natl. Acad. Sci. USA 113 (16), 4518–4523.
Chen, J.E., Chang, C., Greicius, M.D., Glover, M.D., 2015. Introducing co-activation pattern metrics to quantify spontaneous brain network dynamics. Neuroimage 111, 476–488.
Chu, C.J., et al., 2015. EEG functional connectivity is partially predicted by underlying white matter connectivity. Neuroimage 108, 23–33.
Cocchi, L., Zalesky, A., Fornito, A., Mattingley, J.B., 2013. Dynamic cooperation and competition between brain systems during cognitive control. Trends Cogn. Sci. 17, 493–501.
Daducci, A., et al., 2012. The connectome mapper: an open-source processing pipeline to map connectomes with MRI. PLoS One 7 (e48121).
Daducci, A., Dal Palú, A., Descoteaux, M., Thiran, J.P., 2016. Microstructure informed tractography: pitfalls and open challenges. Front. Neurosci. 10, 247.
Dale, A.M., Fischl, B., Sereno, M.I., 1999. Cortical surface-based analysis. I. Segmentation and surface reconstruction. Neuroimage 9, 179–194.
Damoiseaux, J.S., et al., 2006. Consistent resting-state network across healthy subjects. Proc. Natl. Acad. Sci. USA 103 (37), 13848–13853.
Deco, G., Jirsa, V.K., McIntosh, A.R., 2011. Emerging concepts for the dynamical organization of resting-state activity in the brain. Nat. Rev. Neurosci. 12, 43–56.
Deco, G., Tononi, G., Boly, M., Kringelbach, M.L., 2015. Rethinking segregation and integration: contributions of whole-brain modeling. Nat. Rev. Neurosci. 16, 430–439.
Deco, G., Kringelbach, M.L., 2016. Metastability and coherence: extending the communication through coherence hypothesis using a whole-brain computational perspective. Trends Neurosci 39, 125–135.
De Pasquale, F., Della Penna, S., Sporns, O., Romani, G.L., Corbetta, M., 2015. A dynamic core network and global efficiency in the resting human brain. Cereb. Cortex. http://dx.doi.org/10.1093/cercor/bhv185.
De Reus, M.A., van den Heuvel, M.P., 2013. Estimating false positives and negatives in brain networks. Neuroimage 70, 402–409.
De Reus, M.A., van den Heuvel, M.P., 2014. Simulated rich-club lesioning in brain networks: a scaffold for communication andIntegration? Front. Hum. Neurosci. 8 (647).
Fox, P., et al., 2005. The human brain is intrinsically organized into dynamics, anticorrelated functional networks. Proc. Natl. Acad. Sci. USA 102 (27), 9673–9678.
Fries, P., 2005. A Mechanism for cognitive dynamics: neuronal communication through neuronal coherence. Trends Cogn. Sci. 9, 474–480.
Fries, P., 2015. Rhythms of cognition: communication through coherence. Neuron 88, 220–235.
Friston, K.J., 2011. Functional and effective connectivity: a review. Brain Connect 1 (1), 13–36.
Goñi, J., et al., 2013. Exploring the morphospace of communication efficiency in complex networks. PloS One 8 (3), e58070.
Goñi, J., et al., 2014. Resting-brain functional connectivity predicted by analytic measures of network communication. Proc. Natl. Acad. Sci. USA 111, 833–838.
Gonzalez-Castillo, J., et al., 2014. The spatial structure of resting state connectivity stability on the scale of minutes. Front. Neurosci. 8 (138).
Greve, A., Fischl, B., 2009. Accurate and robust brain image alignment using boundary-based registration. NeuroImage 48 (1), 63–72.
Hagmann, P., et al., 2008. Mapping the structural core of human cerebral cortex. PLoS Biol. 6 (e159).
Handwerker, D.A., Roopchansingh, V., Gonzalez-Castillo, J., Bandettini, P.A., 2012. Periodic changes in fMRI connectivity. Neuroimage 6 (63), 1712–1719.
Hansen, E.C.A., Battaglia, D., Spiegler, A., Deco, G., Jirsa, V.K., 2015. Functional connectivity dynamics: modeling the switching behavior of the resting state. Neuroimage 105, 525–535.
Hellyer, P.J., Scott, G., Shanahan, M., Sharp, D.J., Leech, R., 2015. Cognitive flexibility through metastable neural dynamics is disrupted by damage of the structural connectome. J. Neurosci. 35, 9050–9063.
Hindriks, R., et al., 2016. Can sliding-window correlations reveal dynamic functional connectivity in resting-state fMRI? Neuroimage 127, 242–256.
Hinne, M., Heskes, T., Beckmann, C.F., van Gervel, M.A.J., 2013. Bayesian inference of structural brain networks. Neuroimage 66, 543–552.
Holme, P., Saramaki, J., 2012. Temporal networks. Phys. Rep. 519, 97–125.
Honey, C.J., et al., 2009. Predicting human resting-state functional connectivity from structural connectivity. Proc. Natl. Acad. Sci. USA 106, 2035–2040.
Honey, C.J., Thivierge, J.P., Sporns, O., 2010. Can structure predict function in the human brain? Neuroimage 52, 766–776.
Hutchison, R.M., et al., 2013. Dynamic functional connectivity: promise, issues, and interpretations. Neuroimage 80, 360–378.
Jenkinson, M., Bannister, P., Brady, J.M., Smith, S.M., 2002. Improved optimization of the robust and accurate linear registration and motion correction of brain images. Neuroimage 17 (2), 825–841.
Jenkinson, M., Beckmann, C.F., Behrens, T.E., Woolrich, W.M., Smith, S.M., 2012. FSL. Neuroimage 62, 782–790.
Jones, D., 2008. Studying connections in the living human brain with diffusion MRI.

Cortex 44, 936–952.
Jones, D., Knösche, T.R., Turner, R., 2013. White matter integrity, fiber count, and other fallacies: the do's and don'ts of diffusion MRI. Neuroimage 73, 239–254.
Karahanoğlu, F.I., Caballero-Gaudes, C., Lazeyras, F., Van De Ville, D., 2013. Total activation: fmri deconvolution through spatio-temporal regularization. Neuroimage 73, 121–134.
Karahanoğlu, F.I., Van De Ville, D., 2015. Transient brain activity disentangles fMRI resting-state dynamics in terms of spatially and temporally overlapping networks. Nat. Commun. 6 (7751).
Kitzbichler, M.G., Smith, M.L., Christensen, S.R., Bullmore, E., 2009. Broadband criticality of human brain network synchronization. PloS Comput. Biol. 5 (e1000314).
Kivelä, M., et al., 2014. Multilayer networks. J Complex Netw. 2, 203–271.
Laird, A.R., et al., 2011. Behavioral Interpretations of Intrinsic Connectivity Networks. J Cogn. Neurosci. 23, 4022–4037.
Leonardi, N., Van De Ville, D., 2015. On spurious and real fluctuations of dynamic functional connectivity during rest. Neuroimage 104, 430–436.
Lindquist, M.A., 2008. Tha statistical analysis of fMRI data. Stat. Sci. 23 (4), 439–464.
Liu, X., Duyn, H., 2013. Time-varying functional network information extracted from brief instances of spontaneous brain activity. Proc. Natl. Acad. Sci. USA 110, 4392–4397.
Majeed, W., et al., 2011. Spatiotemporal dynamics of low frequency BOLD fluctuations in rats and humans. Neuroimage 2, 1140–1150.
Michel, V., Gramfort, A., Varoquaux, G., Eger, E., Thirion, B., 2011. Total variation regularization for fMRI-based prediction of behavior. IEEE Trans. Med Imaging 30, 1328–1340.
Mišic, B., et al., 2015. Cooperative and competitive spreading dynamics on the human connectome. Neuron 86, 1518–1529.
Mišic, B., et al., 2016. Network-level structure-function relationships in human neocortex. Cereb. Cortex. http://dx.doi.org/10.1093/cercor/bhw089.
Mitra, A., Snyder, A.Z., Blazey, T., Hacker, C.D., Raichle, M.E., 2014. Lag structure in resting-state fMRI. J. Neurophysiol. 111 (11), 2374–2391.
Mitra, A., Snyder, A.Z., Blazey, T., Raichle, M.E., 2015. Lag threads organize the brain's intrinsic activity. Proc. Natl. Acad. Sci. USA 112, E2235–E2244.
Nicosia, V., Tang, J., Musolesi, M., Russo, G., Mascolo, C., Latora, V., 2012. Components in time-varying graphs. Chaos 22 (2), 023101.
Park, H.J., Friston, K., 2013. Structural and functional brain networks: from connections to cognition. Science 342 (6158). http://dx.doi.org/10.1126/science.1238411.
Petridou, N., Gaudes, C.C., Dryden, I.L., Francis, S.T., Gowland, P.A., 2013. Periods of rest in fMRI contain individual spontaneous events which are related to slowly fluctuating spontaneous activity. Hum. Brain Mapp. 34 (6), 1319–1329.
Ponce-Alvarez, A., et al., 2015. Resting-state temporal synchronization networks emerge from connectivity topology and heterogeneity. PLoS Comput. Biol. 11 (e1004100).
Power, J.D., Barnes, K.A., Snyder, A.Z., Schlaggar, Petersen S.E., 2012. Spurious but systematic correlations in functional connectivity MRI networks arise from subject motion. NeuroImage 59 (3), 2142–2154.
Power, J.D., et al., 2014. Methods to detect, characterize, and remove motion artifacts in resting state fMRI. Neuroimage 84, 320–341.
Preti, M.G., Bolton, T.A.W., van de Ville, D., 2017. The dynamic functional connectome: state-of-the-art and perspectives. Neuroimage, (in press).
Prichard, D., 1994. Generating surrogate data for time series with several simultaneously measured variables. Phys. Rev. Lett. 73 (7), 951–954.
Raichle, M.E., 2015. The brain's default mode network. Annu Rev. Neurosci. 38, 433–447.
Senden, M., Deco, G., de Reus, M.A., Goebel, R., van den Heuvel, M.P., 2014. Rich club organization supports a diverse set of funcitonal network configurations. Neuroimage 96, 174–182.
Shen, K., Hutchison, R.M., Bezgin, G., Everling, S., McIntosh, A.R., 2015. Network structure shapes spontaneous functionl connectivity dynamics. J. Neurosci. 35 (14), 5579–5588.
Smith, S.M., et al., 2009. Correspondence of the brain's functional architecture during activation and rest. Proc. Natl. Acad. Sci. USA 106, 13040–13045.
Spadone, S., et al., 2015. Dynamic reconfiguration of human resting-state networks during visuospatial attention. Proc. Natl. Acad. Sci. USA 112, 8112–8117.
Tagliazucchi, E., Balenzuela, P., Fraiman, D., Chialvo, D.R., 2012. Criticality in large-scale brain fMRI dynamics unveiled by a novel point process analysis. Front Physiol. 3 (15).
Tagliazucchi, E., Siniatchkin, M., Laufs, H., Chialvo, D.R., 2016. The voxel-wise functional connectome can be efficiently derived from co-activations in a sparse spatio-temporal point-process. Front. Neurosci. 10 (381).
Telesford, Q.K., Lynall, M.E., Vettel, J., Miller, M.B., Grafton, S.T., Bassett, D., 2016. Detection of functional brain network reconfiguration during task-driven cognitive states. NeuroImage 142, 198–210.
Theiler, J., Eubank, S., Longtin, A., Galdrikian, B., Farmer, J.D., 1992. Testing for nonlinearity in time series: the method of surrogate data. Physica D 58 (1-4), 77–94.
Thomas, C., et al., 2014. Anatomical accuracy of brain connections derived from diffusion MRI tractography is inherently limited. Proc. Natl. Acad. Sci. USA 111, 16574–16579.
Varela, F., Lachaux, J.P., Rodriguez, E., Martinerie, J., 2001. The brainweb: phase synchronization and large-scale integration. Nat. Rev. Neurosci. 2, 229–239.
Yaesoubi, M., Allen, E.A., Miller, R.L., Calhoun, V., 2015. Dynamic coherence analysis of resting fMRI data to jointly capture state-based phase, frequency and time-domain information. NeuroImage 120, 133–142.
Yeo, B.T., et al., 2011. The organization of the human cerebral cortex estimated by intrinsic functional connecitvity. J. Neurophysiol. 106 (3), 1125–1165.
Wedeen, V.J., Hagmann, P., Tseng, W.Y.I., Reese, T.G., Weisskoff, R.M., 2005. Mapping complex tissue architecture with diffusion spectrum magnetic resonance imaging. Magn. Reson. Med. 54, 1377–1386.
Zalesky, A., Fornito, A., Cocchi, L., Gollo, L.L., Breakspear, M., 2014. Time-resolved resting-state brain networks. Proc. Natl. Acad. Sci. USA 111, 10341–10346.
Zalesky, A., Breakspear, M., 2015. Towards a statistical test for functional connectivity dynamics. Neuroimage 114, 466–470.